Biogeosciences Discuss., 12, 10899–10938, 2015
www.biogeosciences-discuss.net/12/10899/2015/
doi:10.5194/bgd-12-10899-2015

Biogeosciences Discussions
Open Access

Air–water fluxes and sources of carbon dioxide in the Delaware Estuary: spatial and seasonal variability

A. Joesoef, W.-J. Huang, Y. Gao, and W.-J. Cai

School of Marine Science and Policy, University of Delaware, Newark, Delaware, USA

Received: 16 June 2015 – Accepted: 19 June 2015 – Published: 13 July 2015

Correspondence to: W.-J. Cai (wcai@udel.edu)

Published by Copernicus Publications on behalf of the European Geosciences Union.

Abstract

Distributions of surface water partial pressure of carbon dioxide (pCO_2) were measured on nine cruises in the Delaware Estuary (USA). The Delaware River was highly supersaturated in pCO_2 with respect to the atmosphere during all seasons while the Delaware Bay was undersaturated in pCO_2 during spring and late summer and moderately supersaturated during midsummer, fall, and winter. While the upper tidal river was a strong CO_2 source ($24.6 \pm 2.2\,mol\,C\,m^{-2}\,year^{-1}$), the bay was a weak source ($1.8 \pm 0.2\,mol\,C\,m^{-2}\,year^{-1}$), the latter of which had a much greater area than the former. In turn, the Delaware Estuary acted as a relatively weak CO_2 source ($2.4 \pm 0.3\,mol\,C\,m^{-2}\,year^{-1}$), which is in great contrast to many other estuarine systems. Seasonally, pCO_2 changes were greatest at low salinities ($0 \leq S < 5$) with pCO_2 values in the summer nearly three-fold greater than those observed in the spring and fall. Undersaturated pCO_2 was observed over the widest salinity range ($7.5 \leq S < 30$) during spring. Near to supersaturated pCO_2 was generally observed in mid- to high salinity waters ($20 \leq S < 30$) except during spring and late summer. Strong seasonal trends in internal estuarine production and consumption of CO_2 were observed throughout both the upper tidal river and lower bay. Comparably, positive correlations between river-borne and air–water CO_2 fluxes in the upper estuary emphasize the significance of river-borne CO_2 degassing to overall CO_2 fluxes. While river-borne CO_2 degassing heavily influenced CO_2 dynamics in the upper tidal river, these forces were largely compensated by internal biological processes within the extensive bay system of the lower estuary.

1 Introduction

While, globally, the surface area of estuaries is only about 4 % that of continental shelves, recent studies have concluded that the carbon dioxide (CO_2) degassing flux from estuarine waters is as large as the CO_2 uptake by the continental shelf (Borges,

BGD
12, 10899–10938, 2015

2005; Borges et al., 2005; Cai et al., 2006; Chen and Borges, 2009; Cai, 2011). Global estuarine waters are estimated to emit 0.10–0.45 Pg C year^{-1} while continental shelves take up 0.20–0.40 Pg C year^{-1} (Borges, 2005; Borges et al., 2005; Cai, 2011; Chen et al., 2013; Regnier, 2013; Laruelle et al., 2015). Such large estuarine CO_2 degassing suggests that much of the terrestrial organic carbon, including that from coastal wetlands, is respired to CO_2 during transport through the estuarine zone, though the relative importance of river supplied CO_2 and organic carbon verses those from the coastal wetlands is debatable (Borges and Abril, 2011; Cai, 2011). In turn, estuarine waters are a major source of CO_2 to the atmosphere, with partial pressures of CO_2 (pCO_2) ranging from 350 to 10 000 µatm and air–water CO_2 fluxes ranging from −5 to 80 mol C m^{-2} year^{-1} (Raymond et al., 1997; Cai and Wang, 1998; Frankignoulle et al., 1998; Borges, 2005; Borges et al., 2006; Borges and Abril, 2011; Cai, 2011).

Although substantial progress has been achieved over the past decade (Borges and Abril, 2011; Chen et al., 2013; references therein), our knowledge of CO_2 degassing fluxes and their controlling processes in estuaries remains insufficient. Globally, the majority of past estuarine CO_2 studies have been conducted on small estuarine systems, which typically have high pCO_2 (Chen and Borges, 2009; Cai, 2011; Borges and Abril, 2011). Of the 62 estuaries compiled in Borges and Abril (2011), only one (the Aby Lagoon) acted as a sink for atmospheric CO_2. Specifically, in the US east coast, high pCO_2 was found in estuaries along the southeastern (Cai and Wang, 1998; Jiang et al., 2008) and northeastern (Salisbury et al., 2008; Hunt et al., 2010) coastal regions. While high pCO_2 was also found in small estuaries along the US Mid-Atlantic coast (Raymond et al., 1997, 2000), only a few estuarine CO_2 studies have been conducted in this region, such as Crosswell et al. (2012) in the Neuse River, NC, Raymond et al. (1997) in Hudson River, NY, and Raymond et al. (2000) in the York River, VA. Thus, there is limited research on CO_2 dynamics in large estuaries or bay systems with long freshwater residence times in the US Mid-Atlantic coast (most notably the Chesapeake and Delaware estuaries). Presumably, these large estuaries have lower pCO_2 than small estuaries or bay systems with rapid freshwater transit times (Borges

BGD
12, 10899–10938, 2015

and Abril, 2011; Cai, 2011). Overall, there is a lack of data and pressing need to synthesize and expand global research to larger estuaries. Furthermore, of past estuarine CO_2 studies, many lack spatial and seasonal coverage of surface water pCO_2 and air–water CO_2 fluxes, making flux estimates highly uncertain. Consequently, because of these and other reasons, there is rising concern that global estuarine CO_2 degassing flux may be overestimated (Cai, 2011).

The Delaware Estuary is composed of a 100 km-long tidal Delaware River and the Delaware Bay (Fig. 1) (Sharp, 2010). With a relatively simple hydrology, the Delaware Estuary is fairly easy to characterize, and because of this, it has served as a model estuary for biogeochemical study (Cifuentes et al., 1988; Sharp et al., 2009). The tidal freshwater portion of the Delaware River passes through the greater Philadelphia area, the sixth largest municipal region of the US, before flowing into the saline Delaware Bay (Fig. 1) (Sharp et al., 2009; Sharp, 2010). In turn, the upper Delaware River is heavily influenced by major industrial activity. In contrast, the Delaware Bay is a large shallow embayment surrounded by partially undeveloped salt marshes (Cifuentes et al., 1988). Unlike in small estuarine systems, the Delaware Estuary is governed by the dynamic interaction between a river dominated upper estuary and an ocean dominated lower bay. This feature, possibly typical for other large estuarine systems, provides us the opportunity to examine how contrasting geographical settings, physical mixing processes, and ecosystem metabolism in an extensive bay system can affect CO_2 gas exchange.

In this paper, we report seasonal distributions of pCO_2 and air–water CO_2 flux in the Delaware Estuary, which was surveyed nine times via various day- to week-long surveys from 2013 through 2014. We further assess the temperature and biological effects on pCO_2 distributions as well as the overall contribution of internal vs. riverine sources on CO_2 inputs to the estuarine system. Finally, we present a summarized pCO_2 distribution over the study area and provide a conceptual model to illustrate the control mechanisms on surface water CO_2 dynamics in the Delaware Estuary.

BGD
12, 10899–10938, 2015

2 Methods

2.1 Field measurements

The Delaware Estuary was surveyed on nine cruises: 08–10 June 2013, 08–15 August 2013, 17 October 2013, 17–22 November 2013, 23–24 March 2014, 03 July 2014, 27 of August to 01 of September 2014, 30 of October to 02 November 2014, and 05 December 2014. Distributions of pCO_2, dissolved inorganic carbon (DIC), total alkalinity (TA), and pH were measured from the mouth of the bay to the near zero salinity of the estuary in five of the nine cruises. During the August and October 2013 cruises, only surface water pCO_2 was measured.

To monitor levels of pCO_2, surface water was directly pumped through an underway pCO_2 analyzer (AS-P2, Apollo Scitech) installed in the shipboard laboratory (Huang et al., 2015). The equilibrated gas was pumped through a water trap (Peltier cooler), which removed most of the water vapor, and then into a drying tube packed with magnesium perchlorate [$Mg(ClO_4)_2$] or Nafion tubing. Surface water CO_2 (mole fraction of dry air [xCO_2]) was measured approximately every one and a half minutes using an underway flow-through system equipped with a non-dispersive infrared (NDIR) spectrometer (Li-Cor Model Li-7000, Lincoln, NE, USA). This LICOR 7000 was calibrated, every 3–6 h, against three or four CO_2 gas standards (151.5, 395.4, 982.6, and 1969 ppm CO_2 in air) referenced against standards traceable to those of the National Institute of Standards and Technology (NIST). Atmospheric xCO_2 was measured every 3–6 h using the same CO_2 system. In order to avoid contamination from the ship's stack gases or other possible sources of air pollution, the inlet of the atmospheric CO_2 pipe was installed on the highest platform in the front of the ship. An on-board Sea-bird thermosalinograph (SBE-45) measured surface water temperature and salinity. To calculate surface water and atmospheric pCO_2 values, all xCO_2 measurements were corrected to 100 % saturation of water vapor pressure and the in situ surface water temperature (Dickson et al., 2007).

BGD
12, 10899–10938, 2015

DIC and TA water samples were collected throughout the salinity gradient. Multiple samples were taken at near salinity zero and at the mouth of the bay to obtain river and ocean end-member values. Samples for DIC and TA measurements were filtered through a cellulose acetate filter (0.45 µm) into 250 mL borosilicate bottles and then fixed with 100 µL of saturated mercury bichloride solution. Afterwards, sample bottles were kept in 4 to 10 °C for future analysis. DIC was determined by acidifying 0.5–1.0 mL samples with phosphoric acid. The extracted CO_2 gas was subsequently quantified via an infrared gas analyzer (AS-C3 Apollo Scitech). TA was measured by Gran titration (Gran, 1952) using the open cell method with a semi-automatic titration system (AS-ALK2, Apollo Scitech) (Cai et al., 2010a; Huang et al., 2012). Both DIC and TA measurements were calibrated against certified reference material (CRM, provided by A.G. Dickson from Scripps Institution of Oceanography) at a precision level of about ±2 µmol kg^{-1} (Huang et al., 2012).

2.2 Air–water CO_2 flux estimation

In this study, air–water CO_2 fluxes (F, mmol m^{-2} day^{-1}) at pixel i of a 0.01 longitude × 0.01 latitude grid were calculated as follows:

$$F_i = k_i \cdot K_{oi} \cdot (pCO_{2(water)i} - pCO_{2(air)i}) \quad (1)$$

where k_i (cm h^{-1}) is the gas transfer velocity of CO_2, K_{oi} is the solubility coefficient of CO_2 (mol L^{-1} atm^{-1}), which can be calculated from in situ temperature and salinity (Weiss, 1974), and $pCO_{2(water)i}$ and $pCO_{2(air)i}$ (µatm) are the partial pressure of CO_2 in the water and the air, respectively. The mean atmospheric xCO_2 during each cruise and the sea surface temperature, salinity, and pressure were used to calculate the $pCO_{2(air)i}$. A positive F value indicates CO_2 transfer from water to the atmosphere.

Generally, two main issues arise when trying to accurately determine air–water CO_2 fluxes in coastal waters: how to accurately represent surface turbulence and obtaining spatial and temporal heterogeneity of pCO_2 distributions. One of the greatest

BGD
12, 10899–10938, 2015

uncertainties when calculating air–water CO_2 fluxes is estimating gas transfer velocities (Wanninkhof et al., 2009). While gas transfer velocities primarily depend on wind regime in the open ocean, in coastal and shallower estuaries it is probably more complicated as other factors such as tidal currents, bottom stress, wave slope, turbidity, surface films, and fetch limitation can also influence gas exchange rates (Raymond and Cole, 2001; Borges et al., 2004; Zappa et al., 2007; Jiang et al., 2008a; Abril et al., 2009). Unfortunately, there have not been many studies on gas transfer velocities in estuaries and researchers must rely on wind speed dependence to estimate gas exchange rates. Moreover, limited research has been conducted at wind speeds less than $4\,m\,s^{-1}$. In turn, quadratic relationships that estimate k often extrapolate to zero at low wind speeds (Wanninkhof et al., 2009). Increasing evidence suggests that k does not approach zero at low wind speeds but rather asymptotes to a finite value due to various external factors such as buoyancy effects, chemical enhancements, and physical mixing processes (McGillis et al., 2001, 2004; Wanninkhof et al., 2009). To avoid gas transfer velocities of zero in river and inland waters where wind speeds are typically low, we adopted the gas transfer relationship as proposed by Wanninkhof et al., (2009):

$$k_{660} = 3 + 0.1 \cdot U_{10} + 0.064 \cdot U_{10}^2 + 0.011 \cdot U_{10}^3 \quad (2)$$

where k_{660} is the gas transfer velocity at the Schmidt number of 660, which can be calculated from in situ sea surface temperature (Wanninkhof, 1992), and U_{10} is the wind speed at 10 m above the water surface. In the Delaware Estuary, during our cruises, monthly area-averaged wind speeds never exceeded $7\,m\,s^{-1}$.

In addition, because the relationship between k and mean wind speeds is nonlinear, temporal distributions of wind speeds influence gas transfer velocities (Wanninkhof, 1992; Wanninkhof et al., 2002). To accurately determine the effect of variability of winds over a month, Wanninkhof (1992) introduced the nonlinearity coefficient of the wind speeds (C_2), which is calculated as follows (Wanninkhof et al., 2002; Jiang et al.,

BGD
12, 10899–10938, 2015

2008b):

$$C_2 = \left(\frac{1}{n}\sum_{j=1}^{n} U_j^2\right) \Big/ U_{\text{mean}}^2 \quad (3)$$

where C_2 is the nonlinearity coefficient for quadratic terms of gas transfer relationships, U_j is the high-frequency wind speed collected at the buoys, U_{mean} is the monthly mean wind speed, and n is the total number of available wind speeds during that month. We used high-frequency wind speed data (measured every six minutes) obtained from four National Oceanic and Atmospheric Administration (NOAA) buoys (LWSD1, CMAN4, SJSN4, and DELD1) to calculate the nonlinearity coefficients at each buoy and extrapolate them to the entire estuary. Using the calculated nonlinearity coefficients, gas transfer relationships were corrected to obtain the most accurate relationship between gas transfer velocities and wind speeds during each month.

In order to calculate area-averaged CO_2 flux throughout the Delaware Estuary, the system was divided into five zones as defined by Sharp et al. (2009), but with the mid-bay split into two regions and now defined as the upper and mid-bay (Fig. 1). Surface water pCO_2, temperature, salinity, wind speed, and pressure were interpolated onto 0.01×0.01 grid. Following the same method as presented in Jiang et al. (2008b), flux F_i at each pixel was calculated:

$$S_i = \frac{\Delta\text{Lon}}{2\pi} \cdot 2 \cdot \pi \cdot R^2 \cdot \left[\sin\left(\text{Lat}_i + \frac{1}{2}\Delta\text{Lat}\right) - \sin\left(\text{Lat}_i - \frac{1}{2}\Delta\text{Lat}\right)\right] \quad (4)$$

where S_i is the total area surrounding pixel i; ΔLon and ΔLat are the longitude and latitude intervals of the grid respectively, Lat_i is the latitude at pixel i, and R is the radius of the earth. The area-averaged CO_2 flux was calculated as followed (Jiang et al., 2008b):

$$F_{\text{area-averaged}} = \frac{1}{S_1 + S_2 + \ldots S_n} \cdot \sum_{i=1}^{n} F_i \cdot S_i \quad (5)$$

BGD
12, 10899–10938, 2015

Because there is no precise method to account for the uncertainties of air–water CO_2 fluxes, we followed the same approach as described in Jiang et al. (2008b). Atmospheric measurements for each cruise and gas transfer velocities of Wanninkhof et al. (2009) and Wanninkhof (2014) were used to estimate standard deviations of the atmospheric CO_2 and CO_2 flux, respectively.

2.3 Temperature normalized pCO_2 estimation

Temperature changes are important as they influence surface water pCO_2 by governing the thermodynamic equilibrium of the inorganic carbon system (Takahashi et al., 1993). If only controlled by temperature change and no other physical (mixing) or biogeochemical changes, pCO_2 in surface seawater would double for every 16 °C increase ($\partial \ln pCO_2/\partial T = 0.0423\,^{\circ}C$) (Takahashi et al., 1993). The temperature constant above determined by Takahashi et al. (1993) works well for open ocean waters with salinities between 34 and 36 as physical mixing with freshwater is generally minor. After temperature normalization, one may attribute the remaining pCO_2 change to non-thermal processes (mostly biological activity but possibly also mixing processes). However, in coastal oceans mixing is often serious and influences the interpretations of observed temperature dependences. For example, Jiang et al. (2008a) found that values of $\partial \ln pCO_2/\partial T$ in river- and marine-dominated estuaries were less (about 0.027–$0.042\,^{\circ}C^{-1}$) than the isochemical seawater constant $0.0423\,^{\circ}C^{-1}$ as in Takahashi et al., (1993). We suggest that a thermodynamic prediction for estuarine water should be used for such comparisons. Calculated temperature derived coefficients are discussed in detail in Appendix A and in Bai et al., (2015). Similar to the results found in Jiang et al. (2008a), temperature derived constants were lower than the isochemical seawater constant $0.0423\,^{\circ}C^{-1}$ determined by Takahashi et al. (1993). Thus, knowing the extensively complex nature of estuarine systems, it is important to note that derived variances in temperature-normalized pCO_2 provide only a relatively simple analysis of seasonal pCO_2 fluctuations due to temperature and biological processes as it neglects

BGD
12, 10899–10938, 2015

the impact that various physical processes, turbulent forces, and tidal mixing scenarios have on pCO_2 dynamics.

Using a similar approach as in Takahashi et al. (2002), we also attempted to separate the temperature effect from other non-thermal effects on seasonal pCO_2 change. We first normalized temperature to the annual mean temperature via the following (Takahashi et al., 2002):

$$(pCO_{2obs} \text{ at } T_{mean}) = (pCO_2)_{obs} \cdot \exp[C_s(T_{mean} - T_{obs})] \quad (6)$$

where T is temperature (°C), C_s is the averaged $\partial \ln pCO_2 / \partial T$ value for the salinity interval, and subscripts "mean" and "observed" indicate the annual mean and observed values, respectively. Through this approach, we attributed any differences between calculated and observed pCO_2 values as a result of biological activity and/or physical mixing processes (non-thermal). Because measured pCO_2 data obtained during each cruise was rarely stationary, data from each survey was binned by salinity (intervals of five salinity units from 0–30) to better isolate and interpret the thermal and non-thermal effects on seasonal pCO_2 fluctuations. Temperature-normalized pCO_2 values during months with no surveys were estimated by linearly regressing data from adjacent months with sample measurements. In contrast, to best analyze the effect of temperature changes on observed pCO_2 values, annual mean pCO_2 values across each salinity interval were used in conjunction with the mean and observed temperatures via the following equation (Takahashi et al., 2002):

$$(pCO_{2mean} \text{ at } T_{obs}) = (pCO_2)_{mean} \cdot \exp[C_s(T_{obs} - T_{mean})] \quad (7)$$

Using this method, we attributed any differences between calculated mean vs. observed pCO_2 values as a result of seasonal temperature changes. To remove the temperature effect from observed in situ pCO_2, the observed pCO_2 values were normalized to a constant temperature of 12.7 °C, which was the annual mean water temperature measured in the Delaware Estuary during 2013 to 2014.

BGD
12, 10899–10938, 2015

2.4 Estuarine and river CO_2 contributions

Due to various CO_2 sources such as the degradation of organic matter, discharge of sewage effluents, soil induced respiration, freshwater runoff, and addition of humic substances, river water flowing into estuarine systems are typically supersaturated in CO_2 with respect to the atmosphere (Raymond et al., 2000; Abril and Borges, 2004; Borges et al., 2006). To investigate the influence of river-borne CO_2 input to overall air–water CO_2 fluxes, we used similar methods as performed in Jiang et al., (2008a). In situ DIC and TA measurements coupled with inorganic carbon dissociation constants were used to calculate dissolved CO_2 concentrations. We first estimated the contribution of the ocean end-member to the estuarine DIC alone as follows (Jiang et al., 2008a):

$$\mathrm{DIC}_{\text{mixing w/o}} = \frac{S_i}{S_{\text{ocean}}} \cdot \mathrm{DIC}_{\text{ocean}} \tag{8}$$

where $\mathrm{DIC}_{\text{mixing w/o}}$ is the DIC concentration after the ocean end-member is diluted by fresh water with zero DIC and S_i and S_{ocean} are in situ and ocean end-member salinities, respectively (Fig. 2a). When DIC inputs from both the river and the ocean end-members were considered, estuarine DIC was estimated using a two end member mixing model as follows (Jiang et al., 2008a):

$$\mathrm{DIC}_{\text{mixing w/R}} = \frac{S_i}{S_{\text{ocean}}} \cdot \mathrm{DIC}_{\text{ocean}} + \left(1 - \frac{S_i}{S_{\text{ocean}}}\right) \cdot \mathrm{DIC}_{\text{river}} \tag{9}$$

where $\mathrm{DIC}_{\text{mixing w/R}}$ is the DIC concentration after mixing of river and ocean end-members and $\mathrm{DIC}_{\text{river}}$ is the river end-member (Fig. 2a). $\mathrm{TA}_{\text{mixing w/o}}$ and $\mathrm{TA}_{\text{mixing w/R}}$ were also estimated using similar equations by replacing DIC with TA (Fig. 2b). Because CO_2 concentrations do not change linearly during mixing, they were estimated using corresponding DIC and TA mixing values (Jiang et al., 2008a). Moreover, since CO_2 concentrations fluctuate with temperature change, an annual mean temperature of 12.7 °C was used in this work. Thus, the CO_2 contribution due to river input ($\Delta[CO_2]_{\text{riv}}$)

BGD
12, 10899–10938, 2015

was estimated as follows:

$$[CO_2]_{riv} = [CO_2]_{mixing\ w/R} - [CO_2]_{mixing\ w/o} \quad (10)$$

Calculated river CO_2 inputs ($[CO_2]_{riv}$) and combined river discharges from the Schuylkill and Delaware Rivers for each month were used to compute river-borne CO_2 fluxes in the upper tidal river.

To further investigate the influence of CO_2 inputs from the river (external) vs. production from within the estuary (internal), we used a similar but modified method as performed in Jiang et al., (2008a). The CO_2 production or its contribution from within the estuarine zone ($[CO_2]_{est}$) was estimated as follows:

$$[CO_2]_{est} = [CO_2]_i - [CO_2]_{mixing\ w/R} + (\tau_i \cdot F_i) \quad (11)$$

where ($[CO_2]_i$) is the in situ CO_2 concentration, τ_i is the flushing time, and F_i is the air–water CO_2 flux. Specifically, ($[CO_2]_i$) was calculated using in situ DIC and TA concentrations and τ_i was estimated using river discharge rates and volume of each region (Table 1) (Sheldon and Alber, 2002). Surveys that did not contain sufficient river end-member DIC and TA measurements were excluded. Alternatively, Eq. (11) suggests that integrated CO_2 degassing ($\tau_i \cdot F_i$) is supported by the deficit or excess CO_2 concentration ($[CO_2]_{mixing\ w/R} - [CO_2]_i$) plus the internal estuarine CO_2 production or consumption ($[CO_2]_{est}$) exhibited across each region.

3 Results

3.1 Hydrographic conditions

Water temperatures were slightly cooler than the ten-year average during March 2014, June 2013, and July 2014, while water temperatures during the rest of the cruises were slightly warmer (Fig. 3a) (USGS gauge 01 463 500). Discharge conditions during each survey were compared with the 30 year average discharges from 1980 to

BGD
12, 10899–10938, 2015

2014 (Fig. 3b) (USGS gauge 01 463 500). The Delaware River discharged was greatest during March 2014 and June 2013. Discharges were smallest during August 2014, October 2013, November 2013, and November 2014. Of the four low-flow months, all of them except for August 2014 had discharge rates less than one standard deviation of the 30 year average.

The surface water salinity distributions confirm the various river discharge conditions recorded throughout each survey (Fig. 4a–i). Salinity < 1.0 was reached on six of the nine cruises (Fig. 4a–c, e, g, and h). The July 2014, August 2013 and October 2013 cruises only transected as far north as the Chesapeake–Delaware Canal (about 39.55° N) (Fig. 1). Salinity < 1.0 (a minimum of 0.98) was only observed during the July 2014 excursion, which had the highest river discharge of the three partial surveys (Fig. 4c). Generally, high salinity waters (25–32.5) were observed in the lower bay and salinities around 20 to 25 in the mid-bay. The upper bay had a much broader scale ranging from salinities 10 to 20 and during the high flow months of March 2014 and June 2013 salinities < 10 were observed (Fig. 4a and b). Salinities did not reach less than 0.25 in the turbidity maximum zone. Salinity distributions in the urban river were limited due to the lack of surveys conducted in this region.

3.2 Surface water pCO_2

Generally, surface water pCO_2 in the Delaware Estuary increased from the ocean to the river end-member with pCO_2 values ranging from about 150 to over 4000 µatm (Fig. 5a–i). Moreover, pCO_2 exhibited strong seasonal variations across both river and bay portions. The most pronounced shifts in surface water pCO_2 were observed within the lower urban river and turbidity maximum river zones of the Delaware River with pCO_2 being lowest in the cool months (March, October, and November) and highest in the warm months (June, July, and August) (Table 1). During all months, the turbidity maximum zone was supersaturated in CO_2 with respect to the atmosphere (atmospheric pCO_2: 375–398 µatm) except during March 2014 due to a strong spring bloom (Fig. 5a). Throughout the summer and early fall, pCO_2 ranged from about 650 µatm

BGD
12, 10899–10938, 2015

to over 4000 µatm across the turbidity and lower urban river zones (Fig. 5b–e). In late fall, pCO_2 dropped to as low as 500 µatm in the turbidity maximum zone and reached 1400 µatm within the lower urban river zone (Fig. 5f–h). However, the decrease in pCO_2 values were not always observed as temperatures cooled. During the December 2014 cruise, surface water pCO_2 values increased across the turbidity maximum zone ranging from about 650 to 1000 µatm (Fig. 5i). As discussed later, this shift in pCO_2 during winter is likely a result of opposing timing of seasonal temperature cycles and respiration vs. that of river discharge rates.

Surface water pCO_2 exhibited strong seasonal variations in the Delaware Bay as well (Fig. 5a–i). In March 2014, most likely due to a strong biological bloom and low temperature (Fig. 3a), the entire bay system (upper, mid-, and lower) was under-saturated in CO_2 with respect to the atmosphere (Table 1). In particular, pCO_2 reached as low as 160 µatm in the mid-bay (Fig. 5a). During the warmer summer months, pCO_2 in the bay remained around 400 to 500 µatm with occasional undersaturation occurring in the mid-bay region (Fig. 5b–e). In August 2014, low pCO_2 ranging from about 200 to 350 µatm was observed throughout much of the mid- and lower bay regions (Fig. 5e). In contrast, during the late fall pCO_2 values were fairly homogenous throughout the mid- and lower bay (400–450 µatm in October 2013 and 2014 and 375–415 µatm in November 2013) and slightly higher pCO_2 occurring in the upper bay (Fig. 5f–h). In December 2014, pCO_2 increased throughout all regions of the bay with pCO_2 values ranging from 500 to 650 µatm (Fig. 5i).

3.3 Air–water CO_2 fluxes

The urban river and turbidity maximum zone served as strong sources of CO_2 to the atmosphere positive during all months (Table 1). Across the upper to lower bay portions of the estuary, uptake of CO_2 from the atmosphere was greatest during spring ranging from $F_{CO_2} = -12.1$ to $-20.0\,\mathrm{mmol\,m^{-2}\,day^{-1}}$ (Table 1). The CO_2 uptake flux was highest in March 2014 in the mid-bay ($-20.0\,\mathrm{mmol\,m^{-2}\,day^{-1}}$), while the highest

BGD
12, 10899–10938, 2015

CO_2 degassing flux occurred in June 2014 in the urban river (144.8 mmol m^{-2} day^{-1}) (Table 1). Air–water CO_2 fluxes in the upper to lower bay regions decreased in early winter (December) to a minimum in early spring (March), followed by an increase to an annual maximum in early summer (June). In the turbidity maximum zone and urban river, area averaged CO_2 fluxes followed the same seasonal decrease in spring and increase in summer but reached an annual minimum in late fall instead of early spring. In December, the mid- and lower bays, which were typically sinks or weak sources of CO_2, exhibited relatively strong CO_2 fluxes to the atmosphere.

3.4 CO_2 distribution across the salinity gradient

To further investigate pCO_2 variations along the Delaware Estuary, we examined distributions of pCO_2 across the salinity gradient. Due to limited area and salinity coverage, surveys conducted in August and October 2013 were excluded for this assessment. In all months, pCO_2 vs. salinity followed a concave upward trend towards the river end-member (Fig. 6). The seasonal variation between pCO_2 values was largest at low salinities around 0 to 5 with pCO_2 values in the summer nearly two-fold greater than those observed in the spring and fall seasons (Fig. 6). In all seasons, pCO_2 was supersaturated with respect to the atmosphere from salinities 0 to 5. In spring, undersaturated pCO_2 was observed over the widest salinity range from 7.5 to 30. In summer, undersaturated pCO_2 was generally not observed except at moderate salinities around 17 to 28 in August. In fall, pCO_2 values were near atmospheric concentrations around mid-salinity waters and were only undersaturated at salinities greater than 25. In winter, pCO_2 values were always supersaturated with respect to the atmosphere across the entire salinity range. While low salinity waters were strong CO_2 sources, proportionally these upper regions ($0 \leq S < 10$) were small in comparison to the total estuarine study area. In turn, their contribution to overall regional flux is minor. Thus, the Delaware Estuary as a whole acts as a relatively weak CO_2 source

BGD
12, 10899–10938, 2015

(2.4 ± 0.3 mol C m^{-2} year^{-1}), which is in great contrast to many river estuaries that are strong CO_2 sources (26 ± 21 mol C m^{-2} year^{-1}) (Borges and Abril, 2011).

3.5 Seasonal variations in temperature normalized pCO_2

Seasonal distributions of pCO_{2obs} at 12.7 °C, which indicate impacts of non-thermal processes (biological and mixing), varied noticeably throughout the year and across salinity intervals (Fig. 7). Typically, pCO_{2obs} at 12.7 °C was greatest during early and mid-winter season (December and January) except in the 0–5 salinity interval (mostly turbidity maximum zone and urban river) when pCO_{2obs} at 12.7 °C reached its maximum in June. Coupled with decreasing flow, in the 0–5 salinity interval, pCO_{2obs} at 12.7 °C decreased from June to an annual minimum in October. In the mid-salinity waters ($5 \leq S \leq 20$), pCO_{2obs} at 12.7 °C decreased from mid-winter to an annual minimum in March, followed by an increase to a secondary maximum in June. In contrast, in the high salinity waters ($20 \leq S \leq 30$) of the lower bay where biological removal of CO_2 was generally strong, annual minimums were observed in August. The annual distribution of pCO_{2mean} at T_{obs}, which indicates the impact of the seasonal thermal cycle, followed typical bell shaped curves across all salinity intervals with the lowest values occurring in winter and an annual maximum occurring in July.

4 Discussion

The seasonal and spatial distributions of estuarine pCO_2 is governed by the dynamic interaction between water temperature, horizontal and vertical mixing processes, biological processes, and CO_2 contributions from the river, ocean, and estuarine zone (Jiang et al., 2008a; Borges and Abril, 2011; Hunt et al., 2014). In the estuarine zone, the addition or removal of CO_2 include net ecosystem metabolism, DIC exchange between intertidal marshes, groundwater inputs, air–water gas exchanges, and other estuarine contributing processes (Jiang et al., 2008a). In the following sections, we eval-

BGD
12, 10899–10938, 2015

uate the impact that seasonal temperature changes and river discharge rates have on surface water pCO_2 distributions, river and estuarine CO_2 inputs, and river-borne CO_2 fluxes throughout the Delaware Estuary.

4.1 Temperature vs. biological effects on pCO_2

Similar to other estuaries (Borges and Abril, 2011), seasonal temperature changes provided a first control on the observed seasonal changes in pCO_{2obs} (low in the winter and high in the summer, Figs. 3a and 7). This is further reflected in the fact that temperature normalized pCO_2 was always higher than in situ pCO_2 in the winter but lower than in situ pCO_2 in the summer (Fig. 7). Presumably, then, seasonal patterns of the temperature normalized pCO_2 reflect how non-thermal processes (mixing and biological) influence in situ pCO_2. For example, in the urban river and turbidity maximum zones ($S < 5$), high pCO_{2obs} at 12.7 °C in the spring and winter may reflect both river inputs and strong respiratory CO_2 production. In the bay, low pCO_{2obs} at 12.7 °C during the warmer months likely reflect biological CO_2 removal. Comparably, pCO_{2mean} at T_{obs} (changes due to the seasonal thermal cycle) trends were opposite to that of pCO_{2obs} at 12.7 °C with lower than pCO_{2obs} values in the winter and higher than pCO_{2obs} values in the summer. These opposing signals suggest that increases in surface water pCO_2 due to winter-to-summer warming are partially compensated by the reduction of surface water pCO_2 due to the biological removal of CO_2 (Takahashi et al., 2002). This is further compensated by elevated CO_2 degassing to the atmosphere during the summer. Similarly, but in the opposite direction, the reduction in surface water pCO_2 due to fall-to-winter cooling is partially compensated by the elevation of surface water pCO_2 due to the biological addition of CO_2 (Fig. 7).

We further examine the relative importance of the temperature and biological effects in each salinity interval by calculating the ratio of ΔpCO_{2temp} to $\Delta pCO_{2bio}(T/B)$ (for methods please refer to Appendix B). Based on our results, temperature was a dominant factor in controlling surface water pCO_2 in low salinity waters ($0 \leq S \leq 10$) (mainly the urban river and turbidity maximum zone) with T/B ratios ranging from 1.30 to 1.68

BGD
12, 10899–10938, 2015

(Table 2). As salinity increased, both $\Delta pCO_{2thermal}$ and $\Delta pCO_{2non-thermal}$ decreased (Table 2). The decrease in $\Delta pCO_{2thermal}$ may be attributed to the reduction in river water temperatures at the ocean end-member (Hunt et al., 2014). In comparison to the upper tidal river, low T/B ratios ranging from 0.69 to 0.80 were observed in mid-salinity waters ($15 \leq S \leq 25$) (mainly the mid- and lower bay) suggesting that pCO_2 distributions in the Delaware Bay are largely governed by biological and/or mixing processes.

4.2 Influence of river-borne CO_2 on estuarine degassing

Positive correlations between river-borne and air–water CO_2 fluxes illustrate the importance of river inputs to CO_2 degassing fluxes (Fig. 8). In the Delaware Estuary, the largest river-borne CO_2 flux was observed during the highest flow month of June 2013 with river CO_2 flux accounting for 119 and 60 % of the overall CO_2 degassing flux in the urban river and turbidity maximum zone, respectively (Fig. 8). Moreover, during the high flow month of March 2014, river-borne CO_2 fluxes exceeded 200 and 150 % of the overall CO_2 degassing fluxes in the urban river and turbidity maximum zone, respectively (Fig. 8). Presumably, the higher river-borne to overall CO_2 fluxes in March are due to the combined influence of increased river discharge coupled with large CO_2 consumption in the estuary (Figs. 3a and 5a). This is consistent with the observed low pCO_2 and high O_2 values (Fig. 5a) (Cai, unpublished data). In contrast, in July and August 2014, air–water CO_2 fluxes exceeded river-borne CO_2 fluxes indicating strong estuarine CO_2 production. Such internal estuarine CO_2 production is most likely due to respiration in the water column, but may also include other inputs such as benthic respiration and net respiration from surrounding intertidal marshes. In turn, while correlations between river-borne and air–water CO_2 fluxes were exhibited, differences between the two fluxes suggest that the input of CO_2 from other estuarine sources is important.

BGD
12, 10899–10938, 2015

4.3 Internal estuarine production vs. river CO_2 input

Our results illustrate that both the river and the estuarine zone contribute to CO_2 inputs in the Delaware Estuary (Fig. 9). Combined river CO_2 input and internal estuarine production were highest in the urban river (87.8 to 255.4 $\mu mol\,L^{-1}$) and smallest in the lower bay (−38.8 to 7.0 $\mu mol\,L^{-1}$) (Fig. 9). In the tidal river, internal estuarine production exhibited clear seasonal trends with CO_2 contributions being lowest in the spring, highest in the summer, and medium in the fall. Strong seasonal trends in internal estuarine production were also observed in the bay regions. During spring and late summer (March and August 2014), internal estuarine CO_2 signals were negative in the mid- and lower bay zones and reached as much as eight folds greater than total river CO_2 inputs, ranging from −22.9 to −100.4 $\mu mol\,L^{-1}$ (Fig. 9). Thus, the majority of river CO_2 input was heavily compensated by the biological removal of CO_2 in the bay waters. In addition, during spring season high CO_2 consumption was also observed in the upper bay with internal estuarine CO_2 signals (−30.7 $\mu mol\,L^{-1}$) exceeding total river CO_2 contribution (25.7 $\mu mol\,L^{-1}$) (Fig. 9). Depending on river discharge rates, the freshwater residence time in the Delaware Estuary ranges from about 40–90 days (Ketchum, 1952). Due to smaller physical sizes, freshwater residence time in the upper tidal river is much shorter (Table 1). Thus, the percentage of river-borne CO_2 in the upper Delaware Estuary is large (Fig. 9), and that percentage decreases in the mid- and lower bays, which have longer residence times and high biological CO_2 removal (Sharp, 1983).

5 Summary and concluding remarks

While the urban river and turbidity maximum zone are strong CO_2 sources in the Delaware Estuary, these upper regions are small in comparison to the bay regions. Thus, overall the Delaware Estuary acts as a relatively weak CO_2 source ($2.4 \pm 0.3\,mol\,C\,m^{-2}\,year^{-1}$). Seasonal temperature cycles influence the rise and fall

BGD
12, 10899–10938, 2015

of surface water pCO_2 throughout the Delaware Estuary, but these effects are partially compensated by opposing cycles of biological removal and addition of CO_2. Moreover, positive correlations between river-borne and air–water CO_2 fluxes in the upper tidal river emphasize the significance of river-borne CO_2 degassing to overall CO_2 fluxes. Such features are typical for rapidly flushing river-dominated estuaries. While river-borne CO_2 degassing fluxes heavily impact CO_2 dynamics throughout the upper Delaware Estuary, these forces are largely compensated by internal biological processes within the extensive bay system of the lower estuary.

Along the eastern Georgia (USA) coast, Jiang et al. (2008a) identified the Altamaha Sound as a river-dominated estuary with CO_2 fluxes driven by river discharge. Comparably, the Kennebec estuary, located on the central Maine (USA) coast, exhibited high river CO_2 inputs and short freshwater residence times (~ 4 days) suggesting that CO_2 sources in the estuary were mainly controlled by the degassing of river-borne DIC (Hunt et al., 2014). The upper Delaware Estuary showed similar results with high river CO_2 contributions and rapid freshwater transit times during all months (Fig. 9 and Table 1). In contrast, in estuaries with long freshwater residence times (i.e. the Delaware Bay and Scheldt estuary), much, if not all, of the river-borne CO_2 is released into the atmosphere (Abril et al., 2000; Borges et al., 2006). In turn, overall CO_2 emission from the estuary is largely controlled by net community production in the mixed layer (ML NCP) (Borges et al., 2006). In the case of the European Scheldt estuary, long freshwater residence time (30–90 days) leads to extensive DIC enrichment in the water column and high CO_2 emissions to the atmosphere (Abril et al., 2000; Borges et al., 2006). Similarly, and in contrast to the rapid flushing Altamaha Sound, Jiang et al. (2008a) identified the marsh surrounded Sapelo Sound as a marine-dominated estuary with CO_2 fluxes driven by seasonal temperature and metabolic cycles.

Due to its extensive geographic size, one may conceptually model the Delaware Estuary, and in some circumstances, other large estuarine systems as being a funnel-shaped estuary. In this case, air–water CO_2 fluxes in the heterotrophic upper estuary are significantly influenced by intense river-borne CO_2 degassing akin to the river-

BGD
12, 10899–10938, 2015

dominated Altamaha Sound and Kennebec estuary. On the other hand, the autotrophic lower estuary is governed by water column biological processes and seasonal temperature cycles akin to the marine-dominated Sapelo Sound and Scheldt estuary (though the Delaware Estuary and other large estuarine systems are on orders of magnitude more productive than smaller marine-dominated estuaries).

While this study serves as the first air–water CO_2 flux product in the Delaware Estuary, there are several limitations. First, the lack of cross-bay transects limits our knowledge of surface water pCO_2 distributions in shallow waters of the bay system. Due to various biological and physical processes (i.e. influence from nearby marshes or estuarine circulation forces), surface water pCO_2 may vary from within the main channel to the perimeters of the estuary even though our preliminary results indicate such lateral gradient is relatively small. Second, a pressing need to conduct more winter and spring surveys exists in order to fully cover seasonal ranges in key properties such as temperature and river discharge rates. Third, more research is needed in the urban and upper river sections of the estuary to better understand CO_2 dynamics throughout the whole estuarine gradient.

Due to increasing urbanization and industrial activities, the biogeochemistry of the Delaware Estuary may respond differently to the rapidly changing environment than it did in the past. The continuation of research cruises on estuarine and coastal margins can provide crucial insight to the physical and biological changes in the past, present, and future ocean systems. Such extensive surveys, collection of carbonate parameters, and comparison of carbonate parameters over time, can significantly broaden our understanding of the processes that govern these coastal zones. In turn, such knowledge can be used to help predict and hopefully regulate the rise of current and future threats to our coastal ocean systems.

BGD
12, 10899–10938, 2015

Appendix A: Temperature derived coefficients

We first derived temperature constants for a general estuarine system using the Excel macro CO2SYS (Pierrot, 2006) and inorganic carbon dissociation constants from Millero et al. (2006) for estuarine waters (S < 30) and from Mehrbach et al. (1973) refit by Dickson and Millero (1987) for high salinity waters ($S > 30$). River and ocean end-members of TA (900 and 2300 $\mu mol\,kg^{-1}$, respectively) and of DIC (960 and 2000 $\mu mol\,kg^{-1}$, respectively) were used. Calculated pCO_2 varied among different temperatures, from 5 to 30 °C, with the largest difference in low salinities (0 to 5) (Fig. A1). In turn, when binning salinities to intervals of 5 units, the greatest variability in temperature constants was observed in salinities 0–5 and 5–10 (Table A1). Averaged values of $\partial \ln pCO_2/\partial T$ for salinity intervals between 0–35 ranged from 0.0332 to 0.0420 $°C^{-1}$ (Table A1).

Appendix B: Temperature and biological effect

Using similar methods as performed in Takahashi et al. (2002), we calculate the thermal effects on surface water pCO_2 in each salinity interval as follows:

$$\Delta pCO_{2\text{thermal}} = (pCO_{2\text{mean}} \text{ at } T_{\text{obs}})_{\max} - (pCO_{2\text{mean}} \text{ at } T_{\text{obs}})_{\min} \quad \text{(B1)}$$

where $(pCO_{2\text{mean}}$ at $T_{\text{obs}})_{\max}$ and $(pCO_{2\text{mean}}$ at $T_{\text{obs}})_{\min}$ are the maximum and minimum $pCO_{2\text{mean}}$ at T_{obs} values, respectively. Likewise, the non-thermal effects (biological and mixing processes) on surface water pCO_2 were calculated as follows (Takahashi et al., 2002):

$$\Delta pCO_{2\text{non-thermal}} = (pCO_{2\text{obs}} \text{ at } 12.7\,°C)_{\max} - (pCO_{2\text{obs}} \text{ at } 12.7\,°C)_{\min} \quad \text{(B2)}$$

where $(pCO_{2\text{obs}}$ at 12.7 °C$)_{\max}$ and $(pCO_{2\text{obs}}$ at 12.7 °C$)_{\min}$ are the maximum and minimum $pCO_{2\text{obs}}$ at 12.7 °C values, respectively. Thus, the relative importance

BGD
12, 10899–10938, 2015

of these effects in each salinity interval can be expressed as the difference between $\Delta pCO_{2thermal}$ and $\Delta pCO_{2non-thermal}$ $(T - B)$ or the ratio of $\Delta pCO_{2thermal}$ to $\Delta pCO_{2non-thermal}(T/B)$.

Acknowledgements. We thank the captains and crew of R/V *Hugh R. Sharp* and R/V *Joanne Daiber* for their support. We appreciate D. L. Kirchman for his supportive comments and discussion. We also thank J. H. Sharp, D. L. Kirchman, G. W. Luther III, J. H. Cohen, and B. J. Campbell for sharing their research cruises and providing us the opportunity to conduct such extensive surveys. The above ships of opportunity cruises were supported by awards from the National Science Foundation (OCE-1 155 385, OCE-1 261 359, and OCE-1 030 306) and the Delaware Sea Grant College Program (RHCE14-DESG). Cai acknowledges UD internal funds for supporting his research.

References

Abril, G. and Borges, A. V.: Carbon dioxide and methane emissions from estuaries, in: Greenhouse Gas Emissions from Natural Environments and Hydroelectric Reservoirs: Fluxes and Processes, Environmental Science Series, edited by: Tremblay, A., Varfalvy, L., Roehm, C., and Garneau, M., Berlin, Heidelberg, New York, 187–207, 2004.

Abril, G., Commarieu, M. V., Sottolichio, A., Bretel, P., and Guérin, F.: Turbidity limits gas exchange in a large macrotidal estuary, Estuar. Coast. Shelf. S., 83, 342–348, 2009.

Bai, Y., Cai, W.-J., He, X., Zhai, W., Pan, D., Dai, M., and Yu, P.: A mechanistic semi-analytical method for remotely sensing sea surface pCO_2 in river-dominated coastal oceans: a case study from the East China Sea, J. Geophys. Res.-Oceans, 120, 2331–2349, 2015.

Borges, A. V.: Do we have enough pieces of the jigsaw to integrate CO_2 fluxes in the coastal ocean?, Estuaries, 28, 3–27, 2005.

Borges, A. V. and Abril, G.: Carbon dioxide and methane dynamics in estuaries, in: Treatise on Estuarine and Coastal Science, edited by: Wolanski, E. and McLusky, D., Academic Press, Waltham, 119–161, 2011

Borges, A. V., Delille, B., Schiettecatte, L.-S., Gazeau, F., Abril, G., and Frankignoulle, M.: Gas transfer velocities of CO_2 in three European estuaries (Randers Fjord, Scheldt, and Thames), Limnol. Oceanogr., 49, 1630–1641, 2004.

BGD
12, 10899–10938, 2015

Borges, A. V., Delille, B., and Frankignoulle, M.: Budgeting sinks and sources of CO_2 in the coastal ocean: diversity of ecosystems counts, Geophys. Res. Lett., 32, 1–4, 2005.
Borges, A. V., Schiettecatte, L.-S., Abril, G., Delille, B., and Gazeau, F.: Carbon dioxide in European coastal waters, Estuar. Coast. Shelf S., 70, 375–387, 2006.
Cai, W.-J.: Estuarine and coastal ocean carbon paradox: CO_2 sinks or sites of terrestrial carbon incineration?, Annu. Rev. Mar. Sci., 3, 123–145, 2011.
Cai, W.-J. and Wang, Y.: The chemistry, fluxes, and sources of carbon dioxide in the estuarine waters of the Satilla and Altamaha Rivers, Georgia, Limnol. Oceanogr., 43, 657–668, 1998.
Cai, W.-J., Wang, Y., and Hodson, R. E.: Acid-base properties of dissolved organic matter in the estuarine waters of Georgia, USA, Geochim. Cosmochim. Ac., 62, 473–483, 1998.
Cai, W.-J., Dai, M., and Wang, Y.: Air–sea exchange of carbon dioxide in ocean margins: a province-based synthesis, Geophys. Res. Lett., 33, 2–5, 2006.
Cai, W.-J., Hu, X., Huang, W.-J., Jiang, L.-Q., Wang, Y., Peng, T.-H., and Zhang, X.: Alkalinity distribution in the western North Atlantic Ocean margins, J. Geophys. Res.-Oceans, 115, 1–15, 2010a.
Cai, W.-J., Luther III., G. W., Cornwell, J. C., and Giblin, A. E.: Carbon cycling and the coupling between proton and electron transfer reactions in aquatic sediments in Lake Champlain, Aquat. Geochem., 16, 421–446, 2010b.
Chen, C.-T. A. and Borges, A. V.: Reconciling opposing views on carbon cycling in the coastal ocean: continental shelves as sinks and near-shore ecosystems as sources of atmospheric CO_2, Deep-Sea Res. Pt. II, 56, 578–590, 2009.
Chen, C.-T. A., Huang, T.-H., Chen, Y.-C., Bai, Y., He, X., and Kang, Y.: Air–sea exchanges of CO_2 in the world's coastal seas, Biogeosciences, 10, 6509–6544, doi:10.5194/bg-10-6509-2013, 2013.
Cifuentes, L. A., Sharp, J. H., and Fogel, M. L.: Stable carbon and nitrogen isotope biogeochemistry in the Delaware Estuary, Limnol. Oceanogr., 33, 1102–1115, 1988.
Crosswell, J. R., Wetz, M. S., Hales, B., and Paerl, H. W.: Air-water CO_2 fluxes in the microtidal Neuse River Estuary, North Carolina, J. Geophys. Res.-Oceans, 117, 1–12, 2012.
Dickson, A. G. and Millero, F. J.: A comparison of the equilibrium constants for the dissociation of carbonic acid in seawater media, Deep-Sea Res., 34, 1733–1743, 1987.
Dickson, A. G., Sabine, C. L., and Christian, J. R.: Guide to best practices for ocean CO_2 measurements, PICES Special Publications, 3, 90–101, 2007.

BGD
12, 10899–10938, 2015

Frankignoulle, M., Abril, G., Borges, A. V., Bourge, I., Canon, C., Delille, B., Libert, E., and Théate, J. M.: Carbon dioxide emission from European estuaries, Science, 282, 434–436, 1998.
Gran, G.: Determination of the equivalence point in potentiometric titrations Part II, Analyst, 77, 661–671, 1952.
Huang, W.-J., Wang, Y., and Cai, W.-J.: Assessment of sample storage techniques for total alkalinity and dissolved inorganic carbon in seawater, Limnol. Oceanogr.-Meth., 10, 711–717, 2012.
Huang, W.-J., Cai, W.-J., Wang, Y., Lohrenz, S. E., and Murrell. M. C.: The carbon dioxide system on the Mississippi River-dominated continental shelf in the northern Gulf of Mexico: 1. Distribution and air–sea CO_2 flux, J. Geophys. Res.-Oceans, 120, 1429–1445, 2015.
Hunt, C. W., Salisbury, J. C., Vandemark, D., and McGillis, W.: Contrasting carbon dioxide inputs and exchange in three adjacent New England estuaries, Estuar. Coast, 34, 68–77, 2010.
Hunt, C. W., Salisbury, J. E., and Vandemark, D.: CO_2 input dynamics and air–sea exchange in a large New England estuary, Estuar. Coast, 37, 1078–1091, 2014.
Jiang, L.-Q., Cai, W.-J., and Wang, Y.: A comparative study of carbon dioxide degassing in river- and marine-dominated estuaries, Limnol. Oceanogr., 53, 2603–2615, 2008a.
Jiang, L.-Q., Cai, W.-J., Wanninkhof, R., Wang, Y., and Lüger, H.: Air–sea CO_2 fluxes on the US South Atlantic Bight: spatial and seasonal variability, J. Geophys. Res., 113, C07019, doi:10.1029/2007JC004366, 2008b.
Ketchum, B. H.: The Distribution of Salinity in the Estuary of the Delaware River, Woods Hole Oceanographic Institution, Woods Hole, Massachusetts, 1952.
Laruelle, G. G., Lauerwald, R., Rotschi, J., Raymond, P. A., Hartmann, J., and Regnier, P.: Seasonal response of air–water CO_2 exchange along the land–ocean aquatic continuum of the northeast North American coast., Biogeosciences, 12, 1447–1458, doi:10.5194/bg-12-1447-2015, 2015.
Mehrbach, C., Culberson, C. H., Hawley, J. E., and Pytkowicz, R. M.: Measurement of the apparent dissociation constants of carbonic acid in seawater at atmospheric pressure, Limnol. Oceanogr., 18, 897–907, 1973.
Millero, F. J., Graham, T. B., Huang, F., Bustos-Serrano, H., and Pierrot, D.: Dissociation constants of carbonic acid in seawater as a function of salinity and temperature, Mar. Chem., 100, 80–94, 2006.

BGD
12, 10899–10938, 2015

McGillis, W. R., Edson, J. B., Hare, J. E., and Fairall, C. W.: Direct covariance air–sea CO_2 fluxes, J. Geophys. Res.-Oceans, 106, 16729–16745, 2001.
McGillis, W. R., Edson, J. B., Zappa, C. J., Ware, J. D., McKenna, S. P., Terray, E. A., Hare, J. E., Fairall, C. W., Drennan, W., Donelan, M., DeGrandpre, M. D., Wanninkhof, R., and Feely, R. A.: Air–sea CO_2 exchange in the equatorial Pacific, J. Geophys. Res.-Oceans, 109, 1978–2012, 2004.
Pierrot, D., Lewis, E., and Wallace, D. W. R.: CO2SYS DOS Program Developed for CO2System Calculations. ORNL/CDIAC-105., Carbon Dioxide Information Analysis Center, Oak RidgeNational Laboratory, US Department of Energy, Oak Ridge, California, 2006.
Raymond, P. A. and Cole, J. J.: Gas exchange in rivers and estuaries: choosing a gas transfer velocity, Estuaries, 24, 312–317, 2001.
Raymond, P. A., Caraco, N. F., and Cole, J. J.: Carbon dioxide concentration and atmospheric flux in the Hudson River, Estuaries, 20, 381–390, 1997.
Raymond, P. A., Bauer, J. E., and Cole, J. J.: Atmospheric CO_2 evasion, dissolved inorganic carbon production, and net heterotrophy in the York River estuary, Limnol. Oceanogr., 45, 1707–1717, 2000.
Regnier, P., Friedlingstein, P., Ciais, P., Mackenzie, F. T., Gruber, N., Janssens, I. A., Laruelle, G. G., Lauerwald, R., Luyssaert, S., Andersson, A. J., Arndt, S., Arnosti, C., Borges, A. V., Dale, A. W., Gallego-Sala, A., Godderis, Y., Goossens, N., Hartmann, J., Heinze, C., Ilyina, T., Joos, F., LaRowe, D. E., Leifeld, J., Meysman, F. J. R., Munhoven, G., Raymond, P. A., Spahni, R., Suntharalingam, P., and Thullner, M.: Anthropogenic perturbation of the carbon fluxes from land to ocean, Nat. Geosci., 6, 597–607, doi:10.1038/ngeo1830, 2013.
Salisbury, J. E., Vandemark, D., Hunt, C. W., Campbell, J. W., McGillis, W. R., and McDowell, W. H.: Seasonal observations of surface waters in two Gulf of Maine estuary-plume systems: relationships between watershed attributes, optical measurements and surface pCO_2, Estuar. Coast. Shelf S., 77, 245–252, 2008.
Sharp, J. H.: The Delaware Estuary: Research as Background For Estuarine Management and Development, Univ. Delaware Sea Grant College Program, Newark, DE, 79–118, 1983.
Sharp, J. H.: Estuarine oxygen dynamics: what can we learn about hypoxia from long-time records in the Delaware Estuary?, Limnol. Oceanogr., 55, 535–548, 2010.
Sharp, J. H., Yoshiyama, K., Parker, A. E., Schwartz, M. C., Curless, S. E., Beauregard, A. Y., Ossolinski, J. E., and Davis, A. R.: A biogeochemical view of estuarine eutrophication: sea-

BGD
12, 10899–10938, 2015

sonal and spatial trends and correlations in the Delaware Estuary, Estuar. Coast, 32, 1023–1043, 2009.

Sheldon, J. E. and Merryl, A.: A comparison of residence time calculations using simple compartment models of the Altamaha River Estuary, Georgia, Estuaries, 25, 1304–1317, 2002.

Takahashi, T., Ólafsson, J., Goddard, J. G., Chipman, D. W., and Sutherland, S. C.: Seasonal variation of CO_2 and nutrient salts over the high latitude oceans: a comparative study, Global Biogeochem. Cy., 7, 843–878, 1993.

Takahashi, T., Sutherland, S. C., Sweeney, C., Poisson, A., Metzl, N., Tilbrook, T., Bates, N., Wanninkhof, R., Feely, R. A., Sabine, C., Olafsson, J., and Nojiri, Y.: Global sea–air CO_2 flux based on climatological surface ocean pCO_2, and seasonal biological and temperature effects, Deep-Sea Res. Pt. II, 49, 1601–1622, 2002.

Wang, Z. A., Cai, W.-J., Wang, Y., and Upchurch, B. L.: A long pathlength liquid-core waveguide sensor for real-time pCO_2 measurements at sea, Mar. Chem., 84, 73–84, 2003.

Wanninkhof, R.: Relationship between wind speed and gas exchange over the ocean, J. Geophys. Res.-Oceans, 97, 7373–7382, doi:10.1029/92jc00188, 1992.

Wanninkhof, R.: Relationship between wind speed and gas exchange over the ocean revisited, Limnol. Oceanogr.-Meth., 12, 351–362, 2014.

Wanninkhof, R., Doney, S. C., Takahashi, T., and McGillis, W. R.: The effect of using time-averaged winds on regional air–sea CO_2 fluxes, in: Gas Transfer at Water Surfaces, Geophysical Monograph Series, edited by: Donelan, M., Drennan, W., Saltzman, E., and Wanninkhor, R., AGU, Washington DC, 351–357, 2002.

Wanninkhof, R., Asher, W. E., Ho, D. T., Sweeney, C., and McGillis, W. R.: Advances in quantifying air–sea gas exchange and environmental forcing, Ann. Rev. Mar. Sci., 1, 213–244, 2009.

Weiss, R. F.: Carbon dioxide in water and seawater: the solubility of non-ideal gas, Mar. Chem., 2, 221–231, 1974.

Zappa, C. J., McGillis, W. R., Raymond, P, A., Edson, J. B., Hintsa, E. J., Zemmelink, H. J., Dacey, J. W. H., and Ho, D. T.: Environmental turbulent mixing controls on air–water gas exchange in marine and aquatic systems, Geophys. Res. Lett., 34, L10601, doi:10.1029/2006GL028790, 2007.

BGD
12, 10899–10938, 2015

Table 1. Flushing time and area-averaged pCO_2 and CO_2 flux (F_{CO_2}) in five of the six zones in the Delaware Estuary during each cruise.

	Mar 2014	Jun 2013	Jul 2014*	Aug 2013*	Aug 2014	Oct 2013*	Oct 2014	Nov 2013	Dec 2014*	Annual Average
Flushing Time (day)										
Lower Bay	14.5	11.7	26.5	23.8	36.2	21.9	18.5	21.9	16.1	21.2
Mid-Bay	29.9	22.9	54.5	38.1	64.1	41.3	30.9	40.0	28.3	38.9
Upper Bay	15.1	13.3	26.6	23.9	32.8	25.5	27.6	27.2	16.6	23.2
Turbidity Maximum Zone	7.6	7.5	11.9	13.3	18.5	19.9	16.1	16.9	11.3	13.7
Urban River	2.5	2.3	3.7	6.1	6.9	6.5	6.5	6.5	5.9	5.2
Average pCO_2 (µatm)										
Lower Bay	230.3	476.9	473.4	384.1	314.5	421.2	404.7	387.3	596.1	409.8
Mid-Bay	198.3	540.2	559.3	529.5	249.5	465.0	421.6	389.9	590.1	438.2
Upper Bay	289.2	918.8	917.2	679.5	469.5	565.8	462.7	434.0	658.3	599.4
Turbidity Maximum Zone	594.6	2086.5	1473.3	1237.0	1101.6	725.8	574.7	541.8	786.4	1013.5
Urban River	868.2	3286.7	2839.2	2176.9	1854.7	879.6	815.6	879.5	877.9	1608.7
Average $F_{CO,2}$ (mmol m^{-2} day^{-1})										
Lower Bay	−15.4	3.8	4.4	3.8	−3.0	1.6	0.8	−1.2	13.5	0.9
Mid-Bay	−20.0	6.8	11.1	10.2	−6.7	4.8	2.0	−1.1	13.5	2.3
Upper Bay	−12.1	25.3	39.5	16.8	5.7	13.0	5.0	3.4	19.7	12.9
Turbidity Maximum Zone	15.9	83.9	63.5	42.2	37.1	21.1	12.3	10.1	26.7	34.8
Urban River	38.3	144.8	123.4	91.6	76.1	40.1	30.2	31.0	32.1	67.5

* Months when surveys did not extend into Urban River.

BGD
12, 10899–10938, 2015

Table 2. Calculated $\Delta pCO_{2thermal}$, $\Delta pCO_{2non-thermal}$, $T - B$, and T/B values for each salinity interval in the Delaware Estuary.

	0–5	5–10	10–15	15–20	20–25	25–30
$\Delta pCO_{2thermal}$ (µatm)	1005	800	635	514	417	431
$\Delta pCO_{2non-thermal}$ (µatm)	773	477	615	635	604	473
$T - B$ (µatm)	232	323	20	−121	−187	−42
T/B	1.30	1.68	1.03	0.80	0.69	0.91

BGD
12, 10899–10938, 2015

Table A1. Averaged temperature coefficients $\partial \ln pCO_2/\partial T$ for each salinity bin. Simulated surface water pCO_2 values at varying salinities were computed using river and ocean end-member TA and DIC values of 900 and 960 µmol kg^{-1} and 2300 and 2000, respectively.

Salinity	Coefficient
0–5	0.0332
5–10	0.0382
10–15	0.0411
15–20	0.0417
20–25	0.0417
25–30	0.0415
30–35	0.0420

BGD
12, 10899–10938, 2015

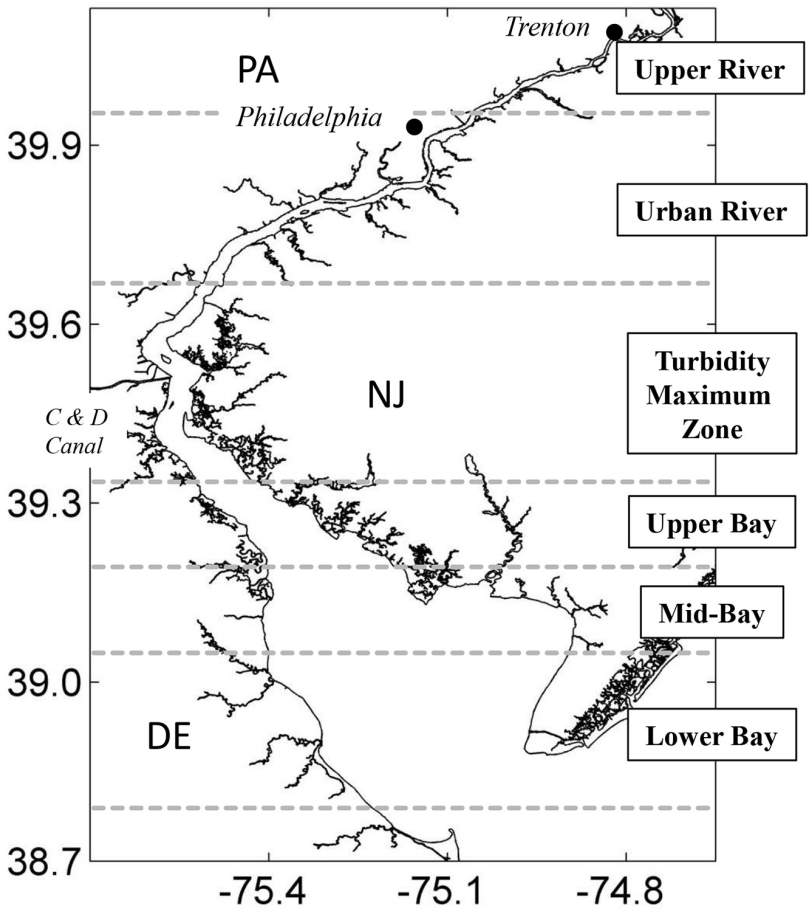

Figure 1. Map of the Delaware Estuary divided into six zones from the head of the tide in Trenton, NJ to the mouth of the bay as defined in Sharp et al. (2009).

BGD
12, 10899–10938, 2015

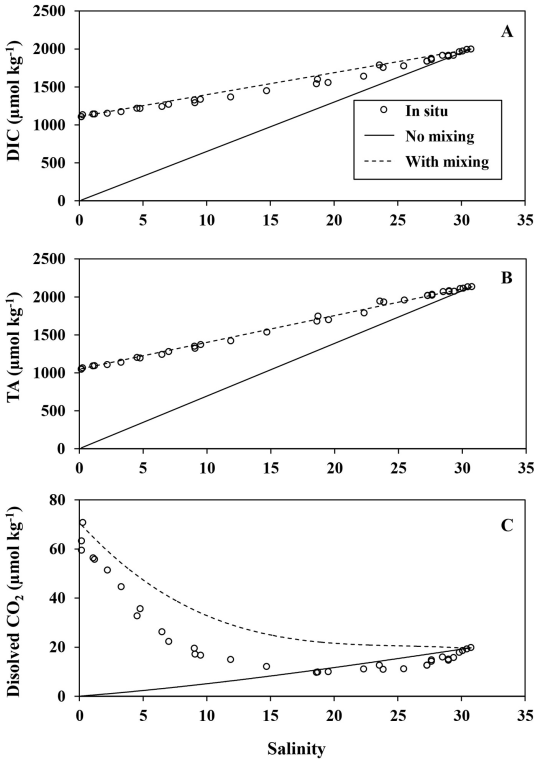

Figure 2. (a) DIC, **(b)** TA, and **(c)** dissolved CO_2 values in the Delaware Estuary during March 2014. Open circles represent in situ concentrations. Solid lines represent values after the ocean end-member is diluted by fresh water with a concentration of zero units. Dotted lines represent concentration after mixing of river and ocean end-members. CO2SYS was used to calculate dissolved CO_2 from measured DIC and TA. In the chemical model of the CO2SYS, NH_3, NH_4^+, and organic matter contribution to TA were not included (Cai et al., 1998, 2010b), which were likely high in low salinity waters. Thus, lower calculated CO_2 than observed CO_2 was expected as the observed TA included other acid-base components.

BGD
12, 10899–10938, 2015

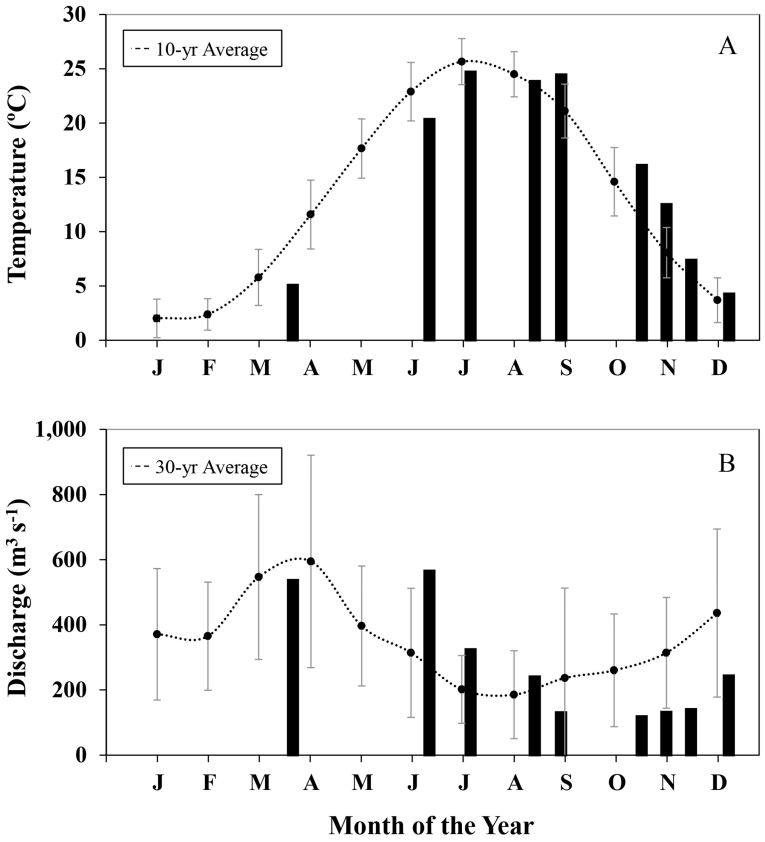

Figure 3. (a) Surface water temperatures and **(b)** Delaware River discharge rates recorded in the Delaware Estuary during each sampling month. Error bars represent standard deviations of the 10 year (2004–2014) and 30 year (1980–2014) monthly averages for surface water temperatures and Delaware River discharge rates, respectively.

BGD
12, 10899–10938, 2015

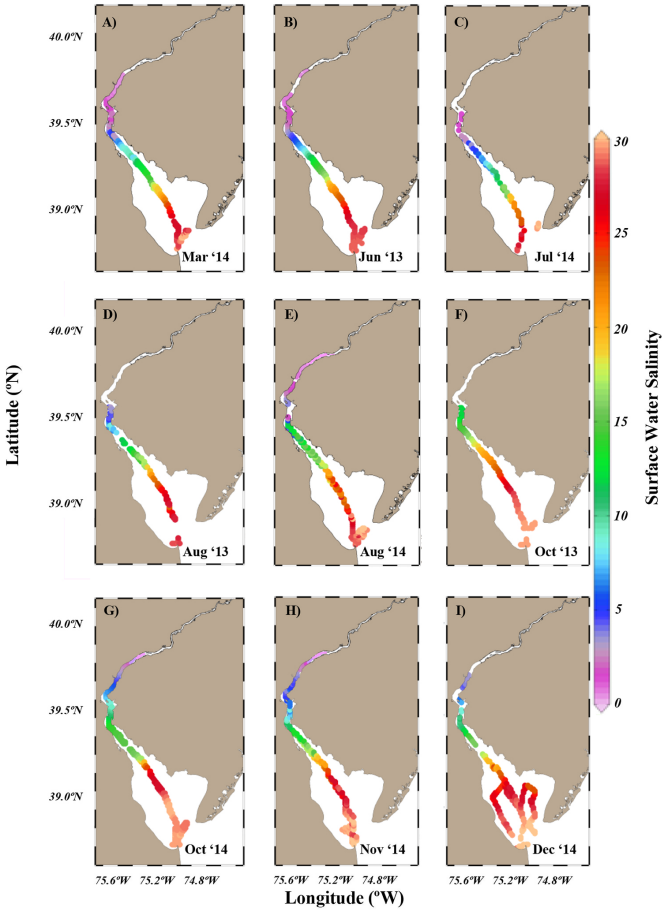

Figure 4. Spatial distributions of surface water salinity in the Delaware Estuary measured during each sampling month.

BGD
12, 10899–10938, 2015

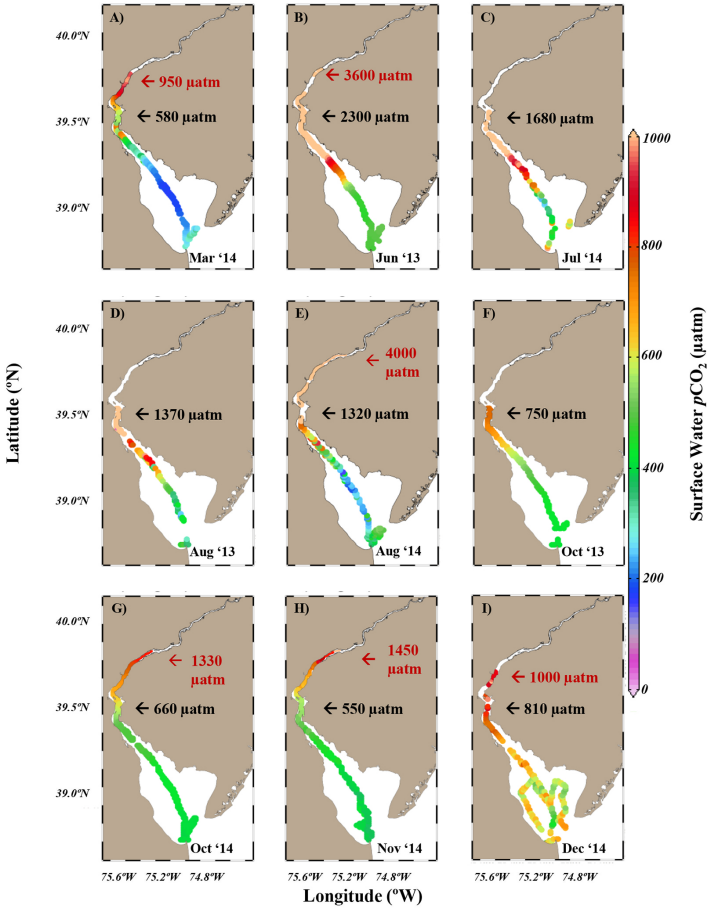

Figure 5. Spatial distributions of surface water pCO_2 in the Delaware Estuary measured during each sampling month. Black and red arrows show surface water pCO_2 values at the Chesapeake–Delaware Canal and the northern end member of each survey, respectively.

BGD
12, 10899–10938, 2015

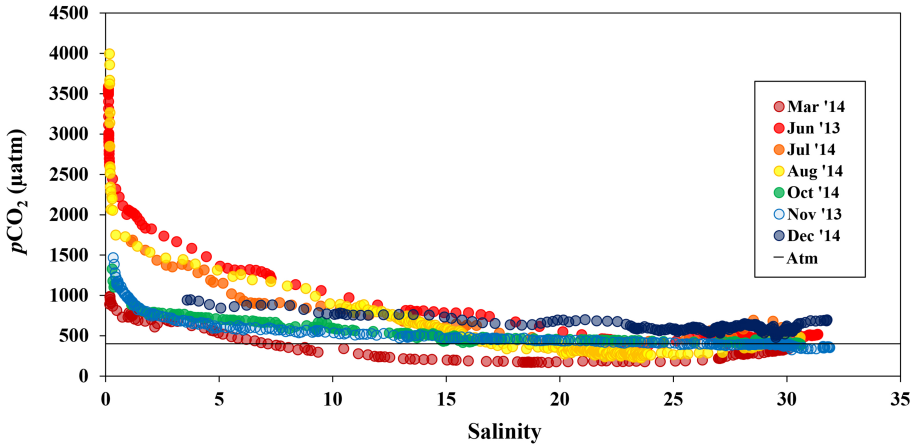

Figure 6. Measured surface water pCO_2 against the salinity gradient during each sampling month in the Delaware Estuary.

BGD
12, 10899–10938, 2015

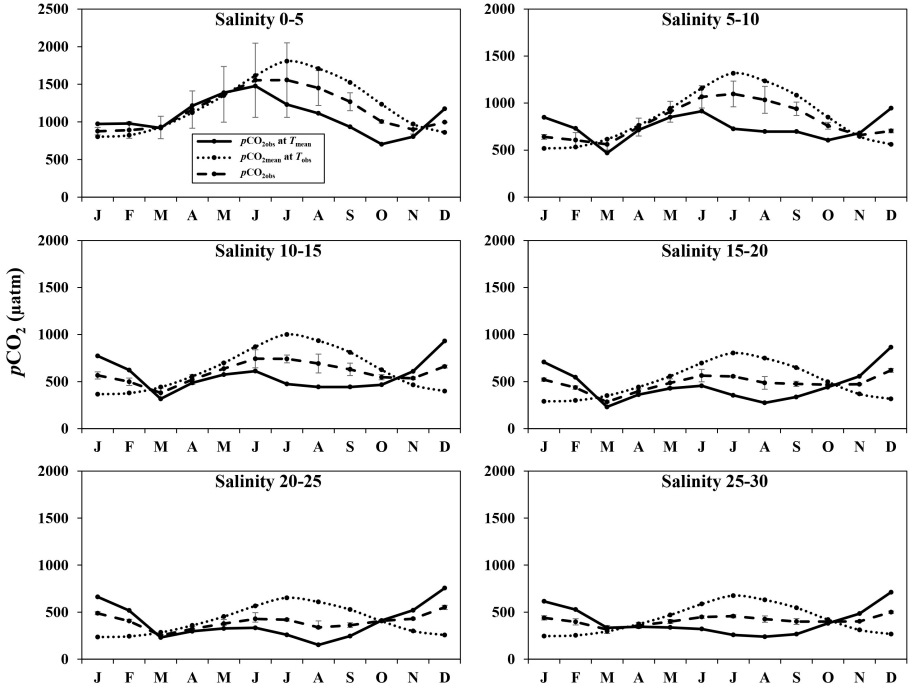

Figure 7. Salinity-binned intervals of temperature-normalized observed pCO_2 values at 12.7 °C, annual mean, area-averaged pCO_2 values at in situ temperature, and observed pCO_2 values in the Delaware Estuary over the year. Error bars represent one standard deviation of the mean value for each month.

BGD
12, 10899–10938, 2015

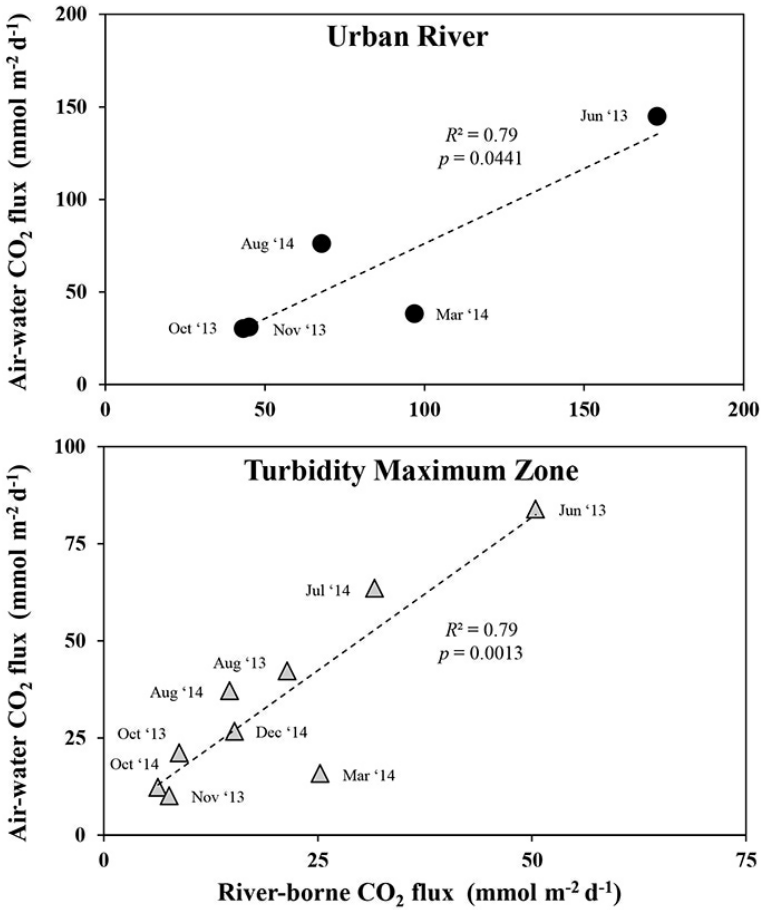

Figure 8. Air–water CO_2 fluxes against river-borne CO_2 fluxes in the urban river and turbidity maximum zone of the Delaware Estuary.

BGD
12, 10899–10938, 2015

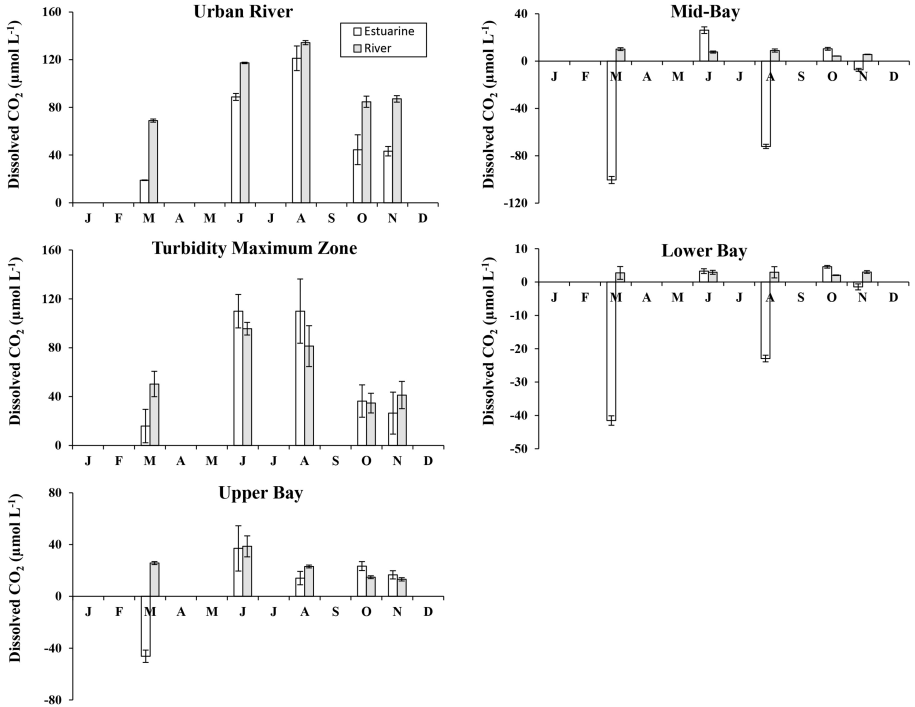

Figure 9. Dissolved CO_2 concentrations (normalized to 12.7 °C, area averaged) due to river inputs and internal estuarine sources in each region of the Delaware Estuary. Error bars represent one standard deviation of the mean value for each month.

BGD
12, 10899–10938, 2015

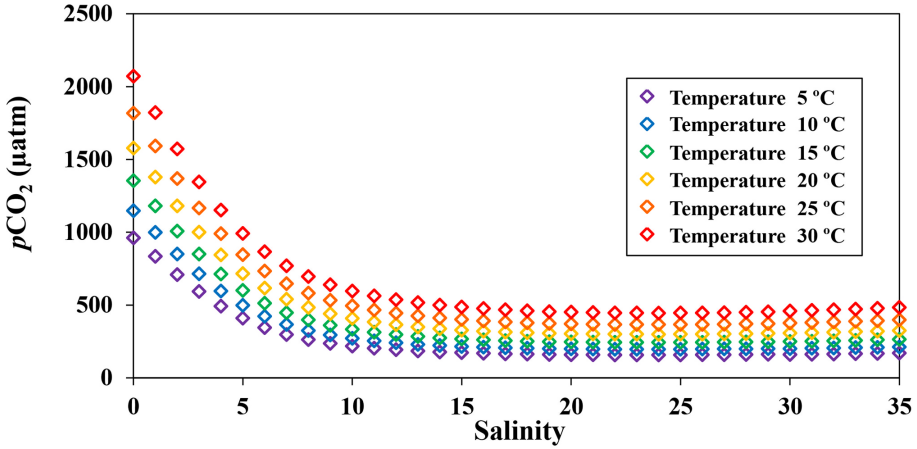

Figure A1. Simulated surface water pCO_2 against salinity grouped by temperature bins. Surface water pCO_2 values were calculated using river and ocean end-member TA and DIC values of 900 and 960 µmol kg^{-1} and 2300 and 2000 µmol kg^{-1}, respectively.

BGD
12, 10899–10938, 2015